Vibrational spectroscopy of thin films and nanostructures by inelastic nuclear resonant scattering

2001 J. Phys.: Condens. Matter 13 7659

(http://iopscience.iop.org/0953-8984/13/34/312)

INSTITUTE OF PHYSICS PUBLISHING JOURNAL OF PHYSICS: CONDENSED MATTER

J. Phys.: Condens. Matter **13** (2001) 7659–7677 PII: S0953-8984(01)26869-6

Vibrational spectroscopy of thin films and nanostructures by inelastic nuclear resonant scattering

R Röhlsberger

Universität Rostock, Fachbereich Physik, August-Bebel-Str. 55, 18055 Rostock, Germany

Received 9 July 2001
Published 9 August 2001
Online at stacks.iop.org/JPhysCM/13/7659

Abstract

The technique of inelastic nuclear resonant scattering is applied to measure the phonon density of states of thin films and nanostructured materials. Interference effects in grazing incidence geometry significantly enhance the inelastic signal from low-dimensional systems. Combined with the oustanding brilliance of modern synchrotron radiation sources this allows one to determine vibrational properties with monolayer sensitivity. An introduction into the basic principles of the method is given, and several experimental examples are discussed.

1. Introduction

The investigation of collective excitations in reduced dimensions by means of advanced x-ray scattering techniques will be an important field in materials science in the future. With further progress in deposition and structuring techniques the variety of materials, as well as their complexity, will strongly increase. Such systems will exhibit great deviations from bulk behavior. Those deviations either limit the desired properties of new materials or they form the basis for a new functionality. A few key areas are identified here:

(a) **Thermal transport in microstructures**: In a confined geometry the vibrational spectrum is altered if the linear dimensions are comparable to the phonon mean free path. This leads to novel features like *phonon zone-folding* in periodic layer structures like superlattices and *phonon confinement* due to the restriction of phonon propagation to certain layers [1]. Such size effects in the vibrational properties will be of particular technical relevance for the thermal properties of thin films that are part of micromechanic and microelectronic devices [2]. Properties like thermal conductivity become more and more critical with increasing power level and decreasing time scales of electronic and mechanical processes in those devices.

(b) **Nanoscale tribology**: The microscopic origin of friction is currently a subject of intense research [3]. Friction is not only a result of structural properties like surface roughness, but also a result of dynamical properties. The vibrational density of states (VDOS) at a particular frequency determines how much energy can be dissipated in that mode. The design of solids with a gap in the VDOS over a critical region of frequencies could prevent energy losses caused by friction. Since these processes are naturally located at buried

interfaces, inelastic x-ray spectroscopy with its great penetration power and high surface sensitivity is the ideal tool to study such systems.

(c) **Smart materials based on lattice instabilities**: 'Smart materials' rely on structural phase transitions, which allow the material to modify the domain structure or the band structure to respond to external parameters like temperature, pressure, electric or magnetic fields [4]. The underlying physics of these phase transitions is intimately related to lattice instabilities with soft phonon modes. In the future new materials with a transformation behaviour based on strongly modified phonon dispersion relations will emerge. Particular examples are ferroelastic and martensitic transformations as the origin of the shape-memory effect that is frequently applied in sensor/actuator systems. Since the efficiency increases with decreasing actuator size there is a strong driving force for further miniaturization into the 100 nm regime. It will be important to determine how the confined geometry of thin films and microstructures affects the fundamental properties of such devices.

The above list indicates that tuning or even tailoring of phononic spectra to specific purposes will be of increasing importance in the future, and a field of *phonon engineering* can be envisaged with many similarities to the common *band gap engineering* of electronic properties. However, a full tunability of these properties will only be possible with a thorough understanding of the underlying processes. The increasing miniaturization of structures requires the further development of existing spectroscopic techniques or the development of new, particularly suited techniques.

The measurement of vibrational properties of thin films is conceptually difficult because neither inelastic neutron scattering nor inelastic x-ray scattering are feasible for such small amounts of material. On the other hand, energy-loss spectroscopy with electrons or He atoms [5] or point-contact methods [6] may be too surface sensitive. Therefore, spectroscopic data on vibrational excitations in thin films are usually obtained by inelastic scattering of infrared or visible light [7]. However, the limited momentum transfer usually prohibits the determination of the full vibrational density of states.

These limitations can be overcome by using x-ray scattering techniques. The availability of high-brilliance, undulator-based synchrotron radiation sources has pushed forward the development of inelastic x-ray scattering techniques with very high energy resolution [8, 9]. Presently, vibrational excitations in solids and liquids are studied with meV-resolution by using backscattering monochromators and analysers [10–14]. While this method probes the coherent inelastic scattering to determine the dispersion of vibrational excitations in condensed matter, a new technique was recently introduced to measure the vibrational density of states via inelastic nuclear resonant scattering [15–18]. This method relies on detection of time-delayed fluorescence photons emitted by decaying Mössbauer nuclei that were excited by synchrotron radiation, i.e. resonant nuclei in the sample are used as energetic analysers. The yield of those fluorescence photons as a function of energy gives a direct measure of the vibrational density of states of the Mössbauer atoms in the sample.

This article describes the basic principles of this technique and its particular application to determine the vibrational properties of thin films. It is intended to give a basic description of the scattering method as well as an introduction into unique applications of this new technique. The first section gives an introduction into the underlying theoretical principles, the determination of the phonon density of states (DOS) from the measured data and the derivation of thermodynamical quantities. The next section then deals with the application of this scattering technique to thin films and describes how the measured signal can be significantly enhanced by interference effects arising from the thin-film geometry. The following sections then give a number of examples where this technique has been applied to thin film systems.

2. Phonon-assisted nuclear resonant absorption

Soon after the discovery of the Mössbauer effect it became clear that nuclear resonant absorption would be a very sensitive tool for the investigation of lattice dynamics. This was put on a theoretical basis by the work of Singwi and Sjölander [19] and Visscher [20]. However, typical phonon energy transfers could not be reached with the conventional Doppler technique and radioactive sources were not strong enough to collect data with sufficient statistics. Hence, the idea was neglected for a long time until synchrotron radiation sources had surpassed the brilliance and spectral flux of radioactive sources by several orders of magnitude. It was in 1995 when three groups almost simultaneously reported the first phonon spectra recorded by inelastic nuclear resonant absorption [15–17]. The experiments were performed at high-brilliance undulator sources with energy resolutions in the range of 6 meV. Since then the technique has made impressive progess and nowadays phonon spectra are routinely recorded with sub-meV energy resolution [21]. Moreover, the enormous brilliance of undulator radiation at third-generation synchrotrons renders this technique sensitive to very small sample volumes like thin films. In the following I will describe the basic features of inelastic nuclear resonant scattering and demonstrate the first application of this technique to study vibrational properties of thin films.

Resonant nuclei in condensed matter provide a very accurate energy reference with a resolution that is only limited by the natural linewidth of the transition. If the energy of the incident radiation is off resonance, excitation of nuclei may be assisted by creation or annihilation of phonons in the sample. Resonance excitation takes place if the energy of the photon plus the energy transfer with the vibrational mode equals the resonance energy. Instead of tuning the incident photon energy relative to the energy of the scattered photon (as is the case in conventional inelastic x-ray scattering [8, 9]), one tunes the incident energy relative to the nuclear resonance. The pulsed time structure of synchrotron radiation permits the use of timing techniques to discriminate the weak delayed nuclear response against the intense electronic scattering. Thus, the energy dependence of the yield of *incoherent* nuclear decay products (conversion electrons or subsequent K-fluorescence photons) gives a direct measure of the number of phonon states in the sample from which the phonon density of states can be derived [16]. An excited nucleus may decay via two channels: radiative decay and internal conversion. The relative probability of these channels is $1/(1+\alpha)$ and $\alpha/(1+\alpha)$, respectively, where α is the conversion coefficient. Since for most Mössbauer isotopes $\alpha > 1$, the dominating channel is internal conversion. Depending on the experimental situation, the following decay channels can be used as the inelastic signal.

(a) **Nuclear resonant fluorescence**: The incident photon is absorbed and reemitted by the nucleus.
(b) **Conversion electron emission**: The excitation energy of the nucleus is transferred to the electron shell, so that an electron is emitted. Due to the small escape depth of the electrons, this method has a potentially high surface sensitivity.
(c) **Atomic fluorescence following internal conversion**: After emission of a conversion electron, the electronic recombination leads to emission of a fluorescence photon. However, if the nuclear transition energy is below the K-edge, K-fluorescence is not possible, as in case of ^{119}Sn [22, 23]. Since L-fluorescence photons are often too low in energy to be efficiently detected, case (a) has to be used then.

A synopsis of the experimental method is shown in figure 1: The incident radiation is monochromatized to an energy width in the meV range by employing subsequent high-order

Bragg reflections in dispersive geometry [24]. Particular crystal arrangements lead to energy resolutions well below 1 meV [21]. The monochromatic radiation hits the thin-film sample under grazing angles. Thin-film interference effects may enhance the yield of fluorescence photons significantly. Moreover, by tuning the angle of incidence, the depth interval can be selected over which the vibrational spectrum of the sample is probed. The incoherent radiation is detected by a time-resolving detector, preferably an avalanche photodiode (APD) [25, 26]. The nuclear fluorescent radiation is discriminated against the prompt radiation by time gating. This requires a bunch pattern in the storage ring with sufficiently large spacing between neighbouring bunches. The energy dependence of the fluorescence yield is obtained by tuning the monochromator energy around the nuclear resonance. After decomposition of the phonon spectrum into the multiphonon contributions, the phonon density of states can be determined from the 1-phonon contribution. In the following I want to elaborate on the quantitative aspects of this method. In an incoherent scattering process the total yield of delayed K-fluorescence

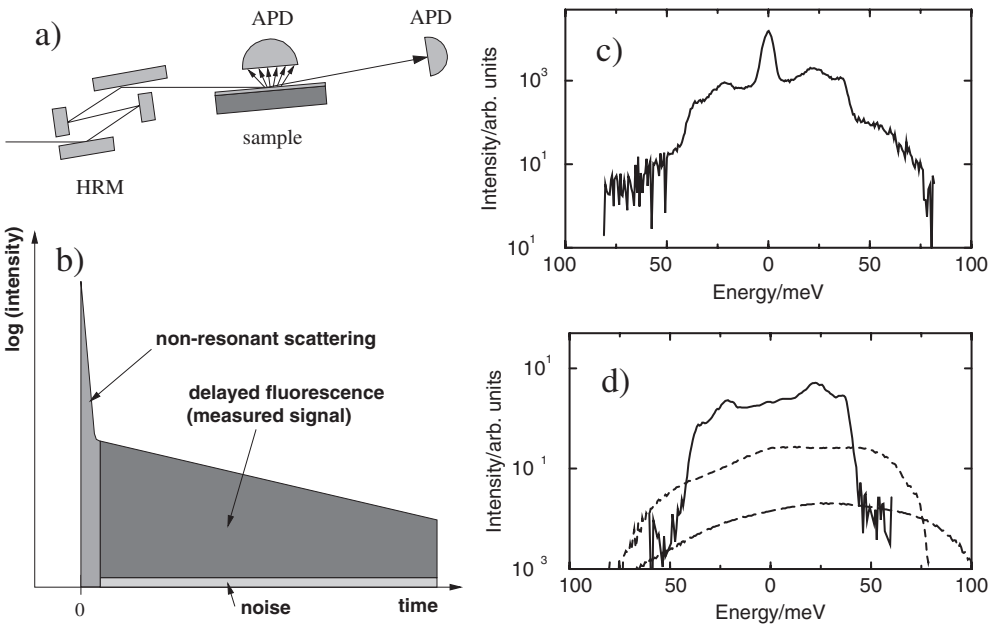

Figure 1. Synopsis of the method of inelastic nuclear resonant scattering: (a) Scheme of the experimental setup with high-resolution monochromator (HRM) and detection of fluorescence quanta over the solid angle with a large-area avalanche photodiode (APD). (b) Time discrimination of the delayed nuclear fluorescence after excitation at $t = 0$. (c) Phonon spectrum of bcc Fe, recorded with an energy resolution of 5 meV. d) 1-, 2- and 3-phonon contributions (solid, dashed and long-dashed lines) as obtained from the deconvolution procedure as outlined in appendix A. The phonon density of states derived from the 1-phonon term according to equation (A.9) is shown in figure 4b.

photons is given by:

$$I(E) = I_0 \, \rho \, \eta_K \, \frac{\Gamma_K}{\Gamma_0} \, \sigma(E) \tag{1}$$

where I_0 is the incident flux, ρ the effective area density of the nuclei, and η_K the K-fluorescence yield. $\Gamma_K/\Gamma_0 = \alpha_K/(1+\alpha)$ is the ratio of the nonradiative (internal conversion) linewidth to the natural linewidth of the nuclear transition. α and α_K are the total and partial internal

conversion coefficients, respectively. $\sigma(E)$ is the cross section for nuclear resonant absorption of a photon with energy E:

$$\sigma(E) = \frac{\pi}{2}\,\sigma(E_0)\,\Gamma_0\,S(E - E_0) \tag{2}$$

where $\sigma(E_0) \equiv \sigma_0$ is the nuclear absorption cross section at the resonance energy E_0. Values of σ_0 for the Mössbauer isotopes are tabulated, e.g., in [27]. $S(E)$ is the normalized probability of absorption per unit energy interval at the energy E. According to Singwi and Sjölander [19] it can be written as:

$$S(\vec{k}_0, E) = \frac{1}{2\pi}\,\mathcal{R}e \int_0^\infty \mathrm{d}t\,\mathrm{e}^{-\mathrm{i}\,E\,t-(1/2)\Gamma_0\,|t|}\,F(\vec{k}_0, t) \tag{3}$$

with

$$F(\vec{k}, t) = \langle\,\mathrm{e}^{-\mathrm{i}\vec{k}\cdot\vec{r}(0)}\,\mathrm{e}^{\mathrm{i}\vec{k}\cdot\vec{r}(t)}\,\rangle \tag{4}$$

where $\mathcal{R}e$ indicates the real part of the integral and the angular brackets stand for averaging over all initial lattice states. The function $F(\vec{k}, t)$ is often referred to as the self-intermediate scattering function. It describes the correlation between the positions of one and the same nucleus at different moments separated by the time interval t. It should be noted that $S(\vec{k}_0, E)$ does not depend on the direction of the wavevector $\vec{k}_S$ of the scattered photon and is thus independent on the momentum transfer $\vec{q} = \vec{k}_S - \vec{k}_0$. However, inelastic nuclear resonant absorption depends on the direction of the incident wavevector $\vec{k}_0$ and is therefore anisotropic in general [28, 29]. The anisotropy vanishes only in the spherical symmetrical (isotropic) limit, i.e., for cubic crystals and polycrystalline samples [1]. This will be discussed in detail in appendix B, because it affects the important question under what conditions the method of nuclear inelastic absorption yields the exact phonon density of states. Since the experiments discussed in this article can be treated in the isotropic limit, I will drop the explicit dependence on $\vec{k}_0$ in the following.

The concept of the self-intermediate scattering function $S(E)$ provides a very general description of the influence of lattice dynamics on resonant absorption. In the approximation of a harmonic lattice, $S(E)$ can be written as a sum over contributions from multiple-phonon excitations as follows [31]:

$$S(E) = f_{LM}\left(\delta_\Gamma(E) + \sum_{n=1}^{\infty} S_n(E)\right) \tag{5}$$

where f_{LM} is the Lamb–Mössbauer factor of the nuclei and $\delta_\Gamma(E)$ is a Lorentzian of width Γ. Since the nuclear linewidth Γ is orders of magnitude smaller than typical phonon energies, this term can be approximated by the Dirac δ-function because $\lim_{\Gamma\to 0}\delta_\Gamma(E) = \delta(E)$.

The function $S(E)$ allows us to extract a number of quantities that characterize the properties of the nuclei in the lattice. They are expressed by the various moments of $S(E)$, often referred to as Lipkin's sum rules [32, 33]:

$$\int E\,S(E)\,\mathrm{d}E = E_R \tag{6}$$

$$\int (E - E_R)^2\,S(E)\,\mathrm{d}E = 4\,E_R\,T \tag{7}$$

$$\int (E - E_R)^3\,S(E)\,\mathrm{d}E = \frac{\hbar^2}{m}\,E_R\,K \tag{8}$$

[1] In this case $F(\vec{k}, t)$ is the spatial Fourier transform of the space-time self-correlation function $G_s(\vec{r}, t)$ introduced by van Hove [30].

where $E_R = E/2mc^2$ is the recoil energy of the free atom, m is the nuclear mass, T is the average kinetic energy of the resonant nuclei and K is the mean force constant of the bound nuclei. The first of these sum rules expresses the remarkable fact that the average energy transfer to the lattice per photon emission is just the recoil energy of the free atom. These sum rules are of great importance for the decomposition of $S(E)$ into the multiphonon contributions. The phonon density of states $D(E)$ is then determined from the single-phonon contribution. A detailed outline of the decomposition procedure is given in appendix A. Once $D(E)$ has been determined, other quantities like lattice specific heat or vibrational entropy can be derived. As will be shown in the following, the method described here offers a unique way to determine such quantities even for systems of reduced dimensionality.

3. Enhanced fluorescence yield due to thin-film interference

The inelastic signal from thin films can be significantly enhanced by interference effects in grazing-incidence geometry. The intensity enhancement results from x-ray standing waves that form above total reflecting boundaries due to superposition of incident and reflected waves [34]. A selection of some typical geometries is shown in figure 2. The right side shows the intensity of the radiation as a function of depth in the sample. At the critical angle, for example, an antinode of the standing wave coincides with the surface, where the intensity peaks with up to four times the incident intensity, see figure 2(a). For the study of thin films, this method becomes particularly effective when the layer under investigation is deposited on a highly reflective substrate, i.e., a material of higher electron density. A substantial intensity enhancement inside the layer is achieved if the layer thickness d is an integer multiple of the standing wave period, because waves that are repeatedly reflected at the boundaries then add up constructively [35–37], see figure 2(b). The normalized intensity I in depth z of a single layer with thickness d on a total reflecting semi-infinite substrate is given by [2] :

$$I(z) = \left|\frac{E(z)}{E_0}\right|^2 = \left|t_{01}\frac{\mathrm{e}^{\mathrm{i}gz} - r_{12}\mathrm{e}^{2\mathrm{i}gd}\mathrm{e}^{-\mathrm{i}gz}}{1 + r_{01}r_{12}\mathrm{e}^{2\mathrm{i}gd}}\right|^2 \tag{9}$$

where g is the z-component of the wavevector in the layer material that is given in the grazing-incidence limit by $g = nk_0\varphi$ with n being the refractive index of the layer material, k_0 the wavenumber of the radiation and φ the angle of incidence. t_{ij} and r_{ij} are the Fresnel transmission and reflection coefficients of the interfaces between adjacent media, where indices $i, j = 0,1,2$ label the vacuum, layer, and substrate, respectively. The intensity enhancement is most pronounced if the film under study is sandwiched between two highly reflecting layers, see figure 2(c). Since the energy transport takes place parallel to the layer boundaries, such layer systems can be regarded as x-ray waveguides [39]. Depending on the film thickness, a certain number of guided modes can be excited, which show up as minima in the rocking curve of the layer system between the critical angles of the layer and the substrate material. Every signal that is derived from the electric field inside the layer can be increased by designing the layer system as an x-ray waveguide and coupling the incident beam into a guided mode by proper adjustment of the angle of incidence.

In the experiments described here, the detector was placed so that mostly fluorescence photons emitted normal to the film plane were counted. Therefore absorption of the fluorescence radiation in the sample can be neglected, and the fluorescence yield is proportional to the integral over the intensity distribution along the z coordinate inside the layer. For a given

[2] This result is derived from equation (4.14) in [38].

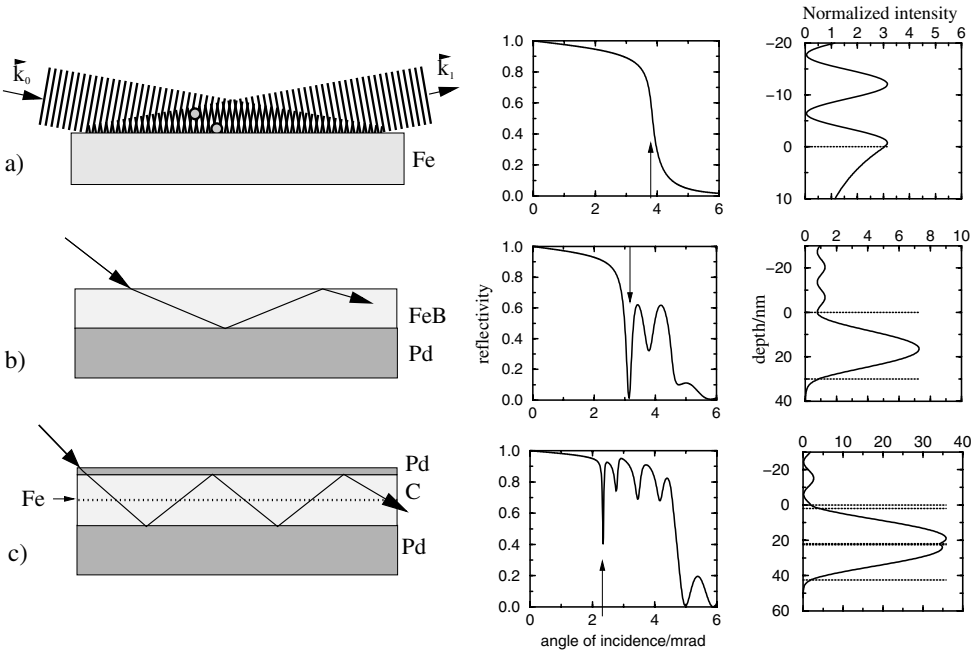

Figure 2. Thin-film interference effects to enhance the fluorecence signal from surfaces and thin films. The graphs show the specular reflectivity of the structures (middle column) and the field intensity as a function of depth (right column). The superposition of incident and reflected waves leads to standing-wave formation (a) above a total-reflecting surface at the critical angle. An antinode of the standing wave coincides with the surface, (b) inside a thin film of FeB on a total-reflecting Pd substrate, (c) inside a Pd/C/Pd sandwich structure that acts as x-ray waveguide structure. Due to a very strong intensity enhancement, this geometry allows to probe the dynamical properties of nanoparticles that are placed in the centre of the C-spacer layer, for example.

deviation E of the incident energy from the nuclear resonance energy, the flux of delayed K-fluorescence photons emitted in the full solid angle is then given by:

$$I(E) = I_0\,\rho\,\sigma_0\,\frac{\eta_K\,\alpha_K}{1+\alpha}\,\frac{\pi}{2}\,\Gamma_0\,S(E)\,\frac{1}{d}\int_0^d I(z)\,\mathrm{d}z \tag{10}$$

where I_0 is the incident flux, ρ is the area density of the nuclei as seen from the direction of the incident beam, σ_0 the nuclear resonant cross section, η_K the fluorescence yield. α and α_K are the total and partial internal conversion coefficients, respectively, Γ_0 is the nuclear level width and $S(E)$ is the inelastic absorption probability per unit of energy. For a single layer on a total reflecting backing, for example, $I(z)$ is given by equation (10).

4. Phonon damping in thin films of polycrystalline Fe

In this experiment we have measured the phonon DOS of ^{57}Fe thin films to identify effects of the confined geometry on the vibrational spectrum [40]. The experiments were carried out at the undulator beamline 3-ID of the APS. The incident radiation was monochromatized to an energy bandwidth of 5.5 meV. Delayed fluorescence photons were counted within a time range of 12–100 ns after excitation with a large area avalanche photodiode (APD) that was

placed right above the film plane. Two films were prepared, consisting of polycrystalline α-Fe (enriched to 95% in ^{57}Fe) with thicknesses of 13 nm and 28 nm, respectively. They were deposited at room temperature by radiofrequency (rf) sputtering in an Ar atmosphere onto a superpolished glass-ceramics substrate (ZERODUR).

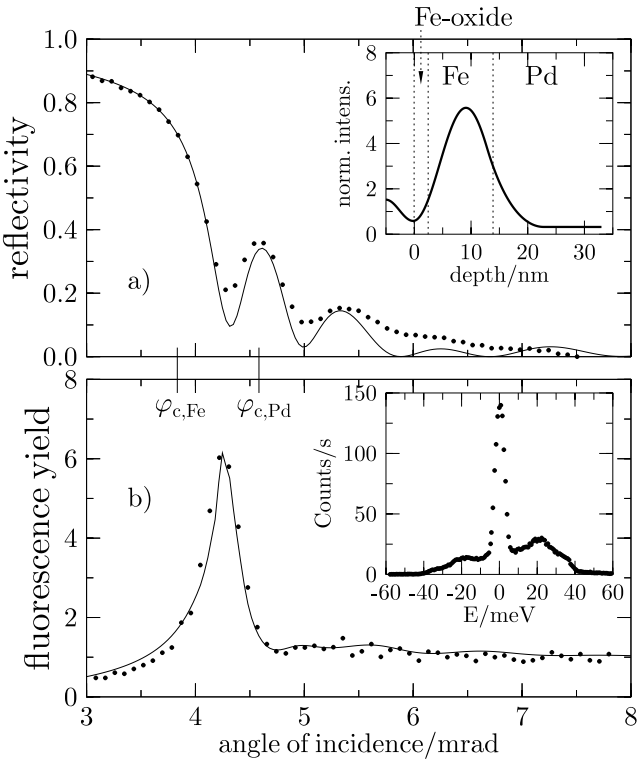

Figure 3. (a) Electronic rocking-curve of 13 nm Fe on Pd. A guided mode is excited at an angle of 4.2 mrad that appears as minimum in the reflectivity between the two critical angles of Fe and Pd. The inset shows the depth dependence of the intensity inside the layer. (b) Angular dependence of the yield of delayed fluorescence from the Fe film, with the photon energy 20 meV above the resonance. The yield peaks at the angle where the guided mode is excited. The inset shows the phonon spectrum that was recorded at this angle. Solid lines are theoretical fits [40].

The 13 nm thick film was deposited onto a 20 nm thick Pd layer to obtain a significant intensity enhancement via x-ray interference in the film, as illustrated in figure 3. The DOS for both films is shown in figures 4(c) and (d). For comparison, the DOS of bulk $\alpha-^{57}$Fe, obtained from a 10 μm thick foil under the same experimental conditions, is shown in figure 4(b). Figure 4(a) shows the DOS of bulk bcc Fe as calculated in a Born–von Karman model with force constants obtained from neutron data [41]. The peak at 35 meV corresponds to longitudinal phonons close to the boundary of the first Brillouin zone, while the two peaks at 23 meV and 27 meV mainly belong to the van Hove singularities of transverse phonons [42]. The most obvious feature in the film DOS is the shape of the peak at 35 meV, which suggests phonon damping in the Fe films.

In order to describe the measured DOS of the films, $D(E)$, we have applied the model of a damped harmonic oscillator (DHO) [43] as was used in a similar study on Fe nanocrystals [44]. This model contains as the only adjustable parameter the quality factor Q that describes the

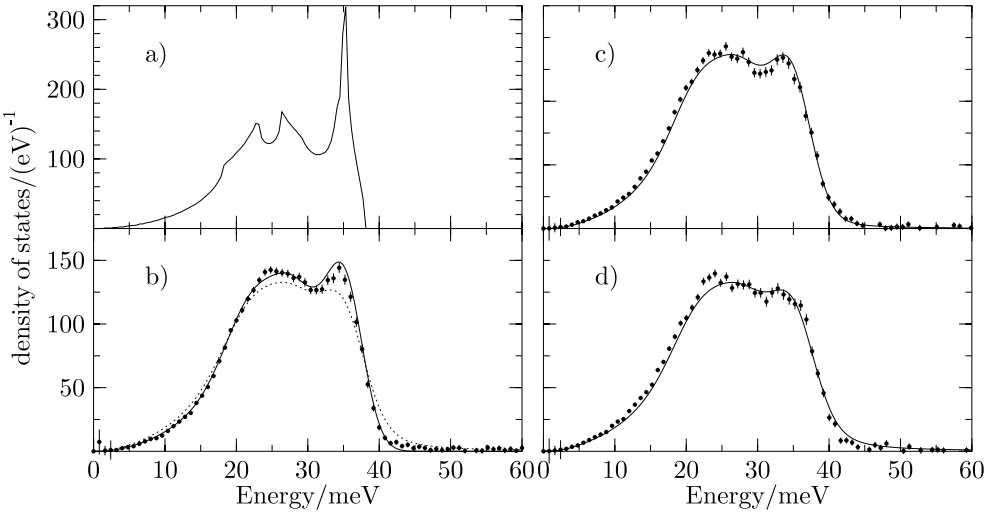

Figure 4. (a) Phonon DOS of bulk Fe, from which the calculations (solid lines) for the following experimental data were derived: (b) DOS of bulk Fe, (c) DOS of 28 nm Fe on ZERODUR, (d) DOS of 13 nm Fe on 20 nm Pd on ZERODUR. The dotted line in (b) corresponds to the solid line in (d). The energy resolution in the experiments was 5.5 meV.

damping of vibrational modes. Comparing the results of the Fe films with that of bulk Fe, the most obvious feature is the shape of the peak at 35 meV, which suggests phonon damping in the Fe films. At each energy E' of the calculated DOS $D_0(E)$ of bulk Fe, we have assumed an energy distribution given by $h(E', E)$ [43]:

$$D(E') = \int_0^\infty h(E', E)\, D_0(E)\, \mathrm{d}E \tag{11}$$

$$h(E', E) = \frac{1}{\pi Q E'} \frac{1}{(E'/E - E/E')^2 + 1/Q^2}. \tag{12}$$

The physical basis for this choice is that the DHO model resembles the inelastic part of the dynamical structure factor of a system with anharmonic interactions that lead to phonon decay [45]. It is frequently applied in inelastic neutron [46] and x-ray scattering [14] and seems to be reasonable if the damping is not too large. In the evaluations presented here, the quality factor Q was the only parameter used to fit the data.

The DOS of the 28 nm thick Fe film shown in figure 4(c) was described with $Q = 25(2)$, while for the 13 nm thick Fe film a value of $Q = 13(1)$ was obtained [40]. For a direct comparison with bulk bcc Fe, the calculated DOS of the 13 nm Fe film is drawn as a dotted line in figure 4(b). The discrepancies between both calculated DOS reveal the features that are introduced by the damping. The high-energy tail is smeared out over a wide range of energies, the peaks due to the van Hove singularities are smoothed, and there is a slight increase of the DOS at low energies, caused by the long tails of the DHO function.

In spite of the good agreement, there remains an excess in the measured DOS over the calculated curve at low energies. Low-energy excitations are often linked to vibrational states in regions with low density or a high degree of disorder. A strong excess of such modes compared to bulk Fe has been observed in nanocrystalline Fe with an average particle size of

10 nm, where a large fraction of the Fe is close to or within surface oxide layers [44]. For the Fe films, the excess at low energies is considerably smaller, probably because the relative contribution from surface and interface regions is small. In the case of the 28 nm film, the thickness of the surface oxide layer is small compared to the total thickness; in the case of the 13 nm film on Pd, the electromagnetic field intensity peaks inside the Fe layer with a relatively small intensity at the interfaces. This is supported by the observation that the DOS of the Fe films does not show modes above 50 meV, which reflects the response of the Fe atoms to high-energy vibrations of O atoms in surface oxides [44].

An enhancement of low energy modes is often found in systems with structural irregularities and is attributed to softening of transverse phonons. The phonon DOS in this energy region for both samples is shown in figure 5, plotted versus E^2. The DOS is to a good approximation quadratic in energy, as expected from the Debye model. The slope indicates the sound velocity in the Fe films to be larger than in the bulk.

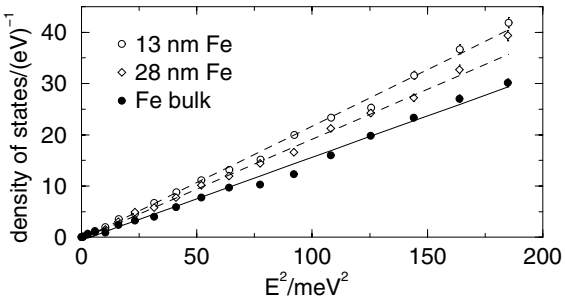

Figure 5. Low-energy region of the phonon DOS of the Fe thin films and bulk Fe from figure 4 plotted against E^2.

The observed differences in the Q values for both films are most likely related to the layer thickness d. Taken as the phonon mean free path, the layer thickness then limits the phonon lifetime in the films. Since the average crystallite size in polycrystalline thin films is in the same range as the layer thickness, this consideration holds also for in-plane phonons scattered at grain boundaries. Stresses originating at the layer boundaries, especially from the surface oxide, may propagate into the layer and give rise to additional scattering processes that shorten the phonon lifetime even more. It should also be noted that in Pd metal there are no phonon modes above 29 meV [42], resulting in a strong confinement of the high-energy modes in the Fe film on Pd.

Although the microscopic origin for the damping could not be discerned here, it is a remarkable fact that the DOS of two different films can be described within the same model with a single parameter. Remaining discrepancies may be due to extra soft modes and slightly different damping of transverse and longitudinal modes. We expect to resolve such effects with recently achieved energy resolutions in the sub-meV range [21]. The measurement of the effective phonon damping may be applied, e.g., to estimate the thermal resistivity of thin films in novel microstructures [2].

5. Lattice dynamics of Fe islands on W(110)

The vibrational properties of clusters, nanoparticles, and nanocrystalline materials have attracted considerable attention recently, because strong deviations from bulk behaviour have

been found [44]. A particular route for production of nanosized particles is the self-organized growth via condensation the gas phase [47], colloidal agglomeration in solution [48] or the formation on single-crystalline surfaces [49]. In the experiment reported here we have investigated nm thick Fe islands on a W(110) surface[3]. The Fe islands, enriched to 95% in ^{57}Fe, were prepared under ultrahigh-vacuum conditions by thermal evaporation. Deposition of a few monolayers and subsequent heating to about 1000 K leads to the formation of separated and well ordered 3D islands [50]. The morphology of these islands is shown in figure 6(a). The surface of the islands is atomically flat. Their long axis points along the W[001] direction. A cross section through a typical Fe island along the W[001] direction is shown in figure 6(c). They are of bcc(110) type with the lattice constant of bulk Fe, as confirmed via x-ray diffraction, shown in figure 6(b). After preparation and characterization, the samples were capped with a 5 nm layer of Ag.

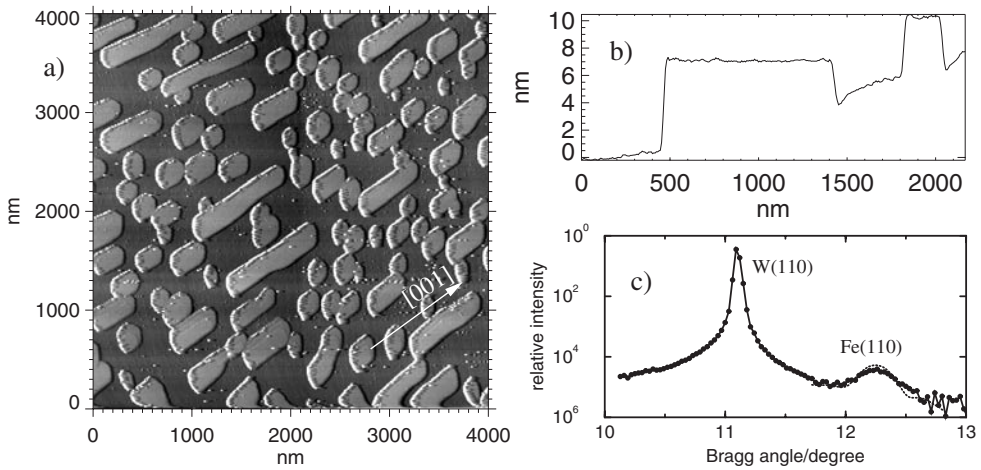

Figure 6. (a) STM image of Fe Islands on W(110). The long axis of the islands points into the W[001] in-plane direction. (b) X-ray diffraction from the (110) reflection of the W substrate and the Fe islands. The dotted line is a theoretical simulation according to the dynamical theory of x-ray diffraction, proving the good crystalline quality of the Fe islands. (c) Cross section through two typical Fe islands along the W[001] direction.

The experiment was carried out at the nuclear resonance beamline ID18 of the ESRF (Grenoble, France). A high-resolution crystal monochromator provided an energy resolution of 4.4 meV. The sample was illuminated in grazing incidence geometry under an angle of 4.5 mrad, close to the critical angle of W. Due to formation of standing waves above the surface, the maximum fluorescence yield is expected at this angular position. A phonon spectrum was recorded by tuning the incident energy over a range of ± 60 meV around the resonance, while monitoring the yield of delayed K-fluorescence photons. The data are shown in figure 7(a), taken during an acquisition time of 12 h. From the phonon spectrum the VDOS was derived according to the procedure described in [16]. The result is shown in figure 7(b). The dashed line represents the VDOS of bulk bcc Fe, convoluted with the same energy resolution function. Pronounced differences appear especially at low phonon energies, where an excess of the island VDOS over the bulk VDOS can be observed. While the damping of vibrational modes at high energies can be described in a phenomenological model [40], the origin of the features

[3] The experiment was performed in close collaboration with K H Meiwes-Broer, J Bansmann and V Senz, University of Rostock.

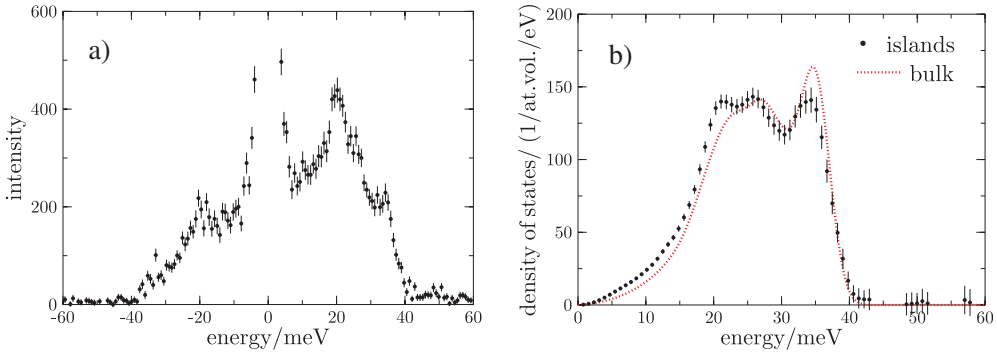

Figure 7. (a) Phonon spectrum of Fe islands on W(110) recorded with an energy resolution of 4.4 meV. (b) Vibrational density of states of Fe islands on W(110) as derived from the phonon spectrum in (a). The dashed line is the calculated phonon DOS of bulk bcc Fe [41, 42], convoluted with the energy resolution function.

at low energies is not fully understood yet. However, similar structures appear also in Fe/Au multilayers where the Fe layer thickness is comparable to the thickness of the Fe islands [51].

6. Vibrational properties of thin-film vitreous $FeBO_3$

The intensity enhancement due to thin film interference can be very efficiently used if the investigated film is sandwiched between two total reflecting layers, as shown in figure 2(c). This has been done in case of a 13 nm thick layer of vitreous $FeBO_3$, produced by sputter deposition, where the fraction of ^{57}Fe in Fe was only 2% (natural abundance). The measurement was possible due to a 10-fold enhancement of the x-ray intensity in a Pd/$FeBO_3$/Pd waveguide structure. The amount of ^{57}Fe in that sample was equivalent to one monolayer. The phonon spectrum is shown in figure 8, recorded at the ESRF with an energy resolution of 4.4 meV. Here the data acquisition time was about 6 hours. The phonon energies in this sample are considerably lower than in the case of crystalline $FeBO_3$ [28]. Although the statistical quality of the data does not allow a derivation of the VDOS, the measurement demonstrates the high sensitivity of the method. With increasing brilliance of modern synchrotron radiation sources and optimized x-ray optics on the beamlines, the signal from single monolayers will be intense enough to study lattice dynamics of nanostructures with atomic resolution [52].

7. Summary and perspectives

In this review I have presented an introduction into the technique of inelastic nuclear resonant scattering of synchrotron radiation with particular emphasis on the vibrational properties of thin films and nanostructures. This method yields the partial VDOS of the Mössbauer atoms in the sample. This opens the unique possibility to selectively determine the vibrational properties of nanostructures that contain the resonant isotope. Due to the inherent isotope specificity of the method there is no need to discriminate against inelastic signals from surrounding materials. A substantial signal enhancement is obtained by making use of x-ray standing waves at surfaces or in thin films. Due to the outstanding brilliance of third-generation synchrotron radiation sources vibrational properties can be determined with high spatial resolution.

While the experiments described here have probed the vibrational properties of the sample in thermal *equilibrium*, the method offers interesting perspectives for probing *non-equilibrium*

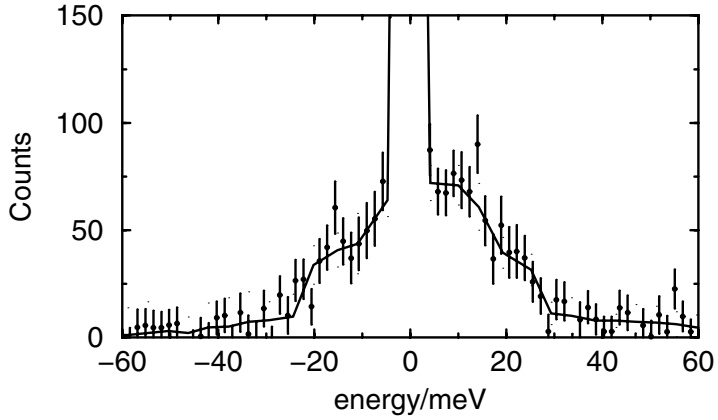

Figure 8. Phonon spectrum of 13 nm vitreous $FeBO_3$ in a Pd/$FeBO_3$/Pd waveguide structure, recorded with an energy resolution of 4.4 meV (from [53]). The solid line is a guide to the eye.

phonon states. Since the incoherent signal reflects the phonon occupation number *at the very moment of excitation* this method is very suitable to be applied in pump-probe experiments. The coupling of the pump pulse is crucial for the spectral distribution of the phonons and their corresponding lifetime. A simple heat pulse will create thermal phonons with lifetimes in the ps range or below. Highly monochromatic phonons with lifetimes of several 100 ns can be created by coupling the laser pulse to impurity resonances that decay via electronic relaxation [54]. If the photon energy of the probe pulse is tuned around the nuclear resonance for a fixed delay between pump and probe pulses, one obtains the phonon spectrum that has developed during this time interval. On the other hand, tuning the time delay between the pump and probe pulse at a fixed off-resonance x-ray energy allows us to monitor the time evolution of particular vibrational states. The investigation of such non-equilibrium phonon states provides valuable information about the thermal transport properties of the sample. An immediate application would be the study of the dynamics of heat-transfer on nanoscopic length scales. Due to the isotopic sensitivity of the absorption process an extremely high spatial resolution can be obtained by the use of probe layers.

Acknowledgments

The experiments described here were performed at the Advanced Photon Source (APS), Argonne National Laboratory, USA and at the European Synchrotron Radiation Facility (ESRF), Grenoble, France. I want to express my thanks to all those, who contributed to the research presented here and provided excellent experimental conditions at these facilities, namely E E Alp, W Sturhahn, T S Toellner, M Hu and J Sutter at the APS and R Rüffer, A I Chumakov and O Leupold at the ESRF. Many thanks also go to K H Meiwes-Broer, J Bansmann, and V Senz for the fruitful collaboration and to E Burkel, A Bernhard and K Quast from the University of Rostock for their continous support. I am also grateful to U Klemradt for stimulating discussions. This work was partially funded by the German BMBF under contract No 05 ST8HRA 0. Use of the Advanced Photon Source was supported by the US Department of Energy, Basic Energy Sciences, Office of Science, under contract No W-31-109-ENG-38.

Appendix A. Extraction of the phonon DOS

In this section I summarize how to extract the phonon density of states $D(E)$ from a measured phonon spectrum. This procedure is basis of a number of evaluation programs and has been described in detail in [55–57]. According to equations (1) and (5), the measured phonon spectrum $I(E)$ can be decomposed into an elastic part that is described by a δ function and an inelastic part $S'(E)$ [4]:

$$I(E) = a\, S'(E) + b\, f_{LM}\, \delta(E). \tag{A.1}$$

The most important aspect for a quantitative data evaluation is the determination of the normalization constants a and b. Unfortunately, due to saturation effects that occur at resonance, those constants are not equal and a common normalization of elastic and inelastic contributions is not possible. Obviously, $b\, f_{LM}$ can be determined from the value $I(0)$ of the measured spectrum. The normalization constant a is determined via Lipkin's sum rule, equation (6) for the first moment of the measured spectrum:

$$a = \frac{1}{E_R} \int I(E)\, E \,\mathrm{d}E. \tag{A.2}$$

The subtraction of the elastic contribution yields the inelastic part of the measured spectrum $I'(E) := a\, S'(E)$. Since $\int S'(E)\,\mathrm{d}E = 1 - f_{LM}$, we immediately obtain for the Lamb–Mössbauer factor:

$$f_{LM} = 1 - \frac{1}{a} \int I'(E)\,\mathrm{d}E \tag{A.3}$$

With this information the measured spectrum can be decomposed into multi-phonon contributions. In the harmonic approximation, the one-phonon contribution $S_1(E)$ is directly related to the phonon density of states $D(E)$:

$$S_1(E) = \frac{E_R\, D(E)}{E\,(1 - e^{-\beta E})} \tag{A.4}$$

The higher-order contributions are given by successive convolutions with the one-phonon term:

$$S_n(E) = \frac{1}{n} \int S_{n-1}(E - E')\, S_1(E')\,\mathrm{d}E' \qquad n > 1 \tag{A.5}$$

Using the convolution theorem, this equation has a very simple expression in Fourier space:

$$\tilde{S}_n(t) = \frac{1}{n}\, \tilde{S}_{n-1}(t)\, \tilde{S}_1(t). \tag{A.6}$$

This recursive relation has the closed solution:

$$\tilde{S}_n(t) = \frac{1}{n!}\, [\tilde{S}_1(t)]^n. \tag{A.7}$$

Thus, taking the Fourier image of equation (5) and performing the summation over the multi-phonon contributions, one obtains:

$$\tilde{S}(t) = f_{LM}\, e^{\tilde{S}_1(t)}. \tag{A.8}$$

Finally, this expression can now be resolved for the one-phonon contribution:

$$S_1(E) = \int \mathrm{d}t\, \mathrm{e}^{-\mathrm{i}\,E\,t}\, \ln\left[\frac{\tilde{S}(t)}{f_{LM}}\right]. \tag{A.9}$$

[4] For a clearer view on the basic concepts, I did not include the instrumental resolution function here. It enters as an additional convolution operation, which is shown below.

This method is known as the Fourier-Log decomposition [58].

Now we include the resolution function $R(E)$ into the formalism, i.e., equation (1) is replaced by:

$$I(E) = \int R(E - E')\,\{aS(E') - b'\,f_{LM}\,\delta(E')\}\,\mathrm{d}E' \tag{A.10}$$

$R(E)$ can be measured very accurately by monitoring the intensity of elastic forward scattering while tuning the incident energy. Including the convolution with $R(E)$ into the above formalism, the expression equation (A.9) for the single-phonon contribution turns into:

$$S_1(E) = \int \mathrm{d}t\,\mathrm{e}^{-i\,E\,t}\,\ln\left[\,1 + \frac{\tilde{I}'(t)}{a\,f_{LM}\,\tilde{R}(t)}\,\right] \tag{A.11}$$

where $\tilde{I}'(t)$ denotes the Fourier image of the measured phonon spectrum with the elastic peak subtracted. The finite width of the resolution function introduces a number of problems that should be discussed here briefly. It is obvious from equation (A.3) that the determination of f_{LM} and the single-phonon contribution critically depends on the subtraction of the elastic peak. Then an assumption has to be made how to describe the region under the elastic peak. In many cases it is reasonable to insert a one-phonon contribution from a Debye solid. However, this procedure has its limits in case of samples with non-Debye behaviour or a strong contribution from multi-phonon terms under the elastic peak. The latter case applies for samples with small f_{LM} and can be cured to some extent by an iterative algorithm [56]. Also the numerical problems that arise from the deconvolution, i.e. the division by $\tilde{R}(t)$, are elaborated in [56].

Once $S_1(E)$ has been obtained, the phonon density of states $D(E)$ can be obtained via equation (A.4). Taking the condition of detailed balance into account, i.e.,

$$S_1(E) = \mathrm{e}^{-\beta\,E}\,S_1(-E) \tag{A.12}$$

that is independent of the material, one can use both wings of the phonon spectrum to determine $D(E)$. The result is:

$$D(E) = \frac{E}{E_R}\,(\,S_1(E) + S_1(-E)\,)\,\tanh\left(\frac{\beta E}{2}\right) \qquad \text{with} \qquad E \geqslant 0. \tag{A.13}$$

Once $D(E)$ has been determined for a particular material, a number of thermodynamic quantities can be derived. As a first example we consider the phonon contribution to the lattice specific heat. The contribution of lattice excitations to the internal energy is given by:

$$U = N \int E\,n(E)\,D(E)\,\mathrm{d}E \tag{A.14}$$

where N is the number of particles and $n(E) = 1/(\mathrm{e}^{E/k_BT} - 1)$ is the Bose occupation number. From this expression the lattice specific heat follows immediately:

$$c_v(T) = \frac{\mathrm{d}U}{\mathrm{d}T} = \frac{N}{k_BT^2}\int_0^\infty E^2\,e^{E/k_BT}\,n(E)^2\,D(E)\,\mathrm{d}E \tag{A.15}$$

Another thermodynamic quantity derived from the VDOS is the vibrational entropy:

$$S_{vib}(T) = R\int_0^\infty D(E)\;[E\,n(E)/k_BT + \ln(1 + n(E))]\;\mathrm{d}E. \tag{A.16}$$

Recent experiments indicate that the relative stability of the ordered and the disordered states of a compound may be significantly affected by their difference in vibrational entropy [59].

Thus, changes in vibrational entropy can be important for the thermodynamics of solid-state phase transitions.

Summarizing, the partial VDOS can be determined from inelastic nuclear resonant scattering almost model-independent. The only assumption made here was that of an isotropic, harmonic lattice. Since the scattering process is fully incoherent, the density of states can be extracted without any approximation or correction for coherent scattering processes. This was investigated in detail by Sturhahn and Toellner [60] who showed that those contributions do not exceed 0.001 of the incoherent channel in case of ^{57}Fe.

It is interesting to compare inelastic nuclear resonant scattering with incoherent inelastic neutron scattering. The data evaluation procedure to extract the VDOS from the measured data is basically the same. In the case of neutron scattering, however, it can be difficult to obtain the exact VDOS directly, in particular if the elements under investigation do not exhibit a significant incoherent scattering cross section, as is the case for Fe. It is the advantage of inelastic nuclear resonant absorption detected via fluorescence to be a fully incoherent process. Therefore, this technique may complement inelastic neutron scattering in many cases. An instructive comparison between both scattering techniques can be found, e.g., in [61] for the investigation of the vibrational properties of quasicrystals.

Appendix B. The exact phonon density of states and the isotropic limit

Inelastic nuclear resonant absorption yields the partial phonon density of states, projected on the direction of the incident beam [29]:

$$\tilde{D}(E,\vec{s}) = \frac{1}{(2\pi)^3}\frac{V}{N_R}\sum_m\sum_j\int \mathrm{d}\vec{q}\,\delta(E-\hbar\omega_j(\vec{q}))\,|\vec{s}\cdot\vec{e}_{j,m}(\vec{q})|^2. \tag{B.1}$$

This differs from the exact phonon density of states that is defined as [62]:

$$D(E) = \frac{1}{(2\pi)^3}\frac{V}{3N}\sum_j\int \mathrm{d}\vec{q}\,\delta(E-\hbar\omega_j(\vec{q})). \tag{B.2}$$

Here, V is the volume of the unit cell and N and N_R are the total number of atoms and the number of resonant atoms in the unit cell, respectively. The indices m and j are used to label the resonant atoms in the unit cell and the vibrational modes, respectiveley. Accordingly, $\vec{e}_{j,m}(\vec{q})$ is the polarization vector of the vibrations of the mth resonant atom and the jth vibrational mode with wavevector $\vec{q}$. $\vec{s}$ is the unit vector along the direction of the incident beam. One notices that $\tilde{D}(E,\vec{s})$ differs from the exact density of states $D(E)$ because the contributions from the vibrational modes of the resonant atoms are weighted by the projections of their polarization vectors on the direction of the incident beam. However, there are two important cases where inelastic nuclear scattering yields the exact phonon density of states of the sample. These are:

- single crystals with a cubic Bravais lattice, and
- polycrystals with an arbitrary monoatomic lattice.

In these cases the inelastic absorption appears to be isotropic, as shown in the following.

Appendix B.1. Single-crystalline systems

To discuss the general anisotropic case we introduce the second-rank Cartesian tensor:

$$T^{\mu\nu}(E) = \frac{1}{(2\pi)^3}\frac{V}{N_R}\sum_m\sum_j\int \mathrm{d}\vec{q}\,\delta(E-\hbar\omega_j(\vec{q}))(\vec{e}_{j,m})_\mu\,(\vec{e}_{j,m})^*_\nu \tag{B.3}$$

With this definition the projected DOS can be written as a quadratic form:

$$\tilde{D}(E,\vec{s}) = \sum_{\mu}\sum_{\nu} s_\mu\, T^{\mu\nu}(E)\, s_\nu \tag{B.4}$$

Any such tensor can be decomposed into its trace T, an antisymmetric part A_κ and a traceless, symmetric part $S^{\mu\nu}$ [63], i.e.,

$$T^{\mu\nu} = \frac{1}{3}\delta_{\mu\nu}T + A_\kappa + S^{\mu\nu}. \tag{B.5}$$

These three quantities transform in the same way as the spherical harmonics of order 0, 1 and 2, respectively. As the antisymmetric part does not contribute to the quadratic form in equation (B.4), we have to consider just two contributions. While the trace T is invariant under rotations in space, the symmetric part contains the anisotropies [64]:

$$s_\mu\, S^{\mu\nu}\, s_\nu = A^{(p)}\, Y_{20}(\Theta,\varphi) + A^{(a)}\,\mathrm{Re}[Y_{22}(\Theta,\varphi)] \tag{B.6}$$

where the polar anisotropy $A^{(p)}$ and the azimuthal anisotropy $A^{(a)}$ are determined by the rotational symmetry of the crystal. These anisotropies vanish for all cubic Bravais lattices. In the other Bravais lattices these anisotropies are nonzero [64], so that inelastic nuclear absorption is generally anisotropic, as has been shown in the case of $FeBO_3$ [28]. However, an anisotropic crystal structure does not necessarily imply anisotropic nuclear absorption; the latter may vanish due to the specific basis of the unit cell. For example, no anisotropy in nuclear inelastic scattering has been found for hematite (Fe_2O_3), although it has the same space group as $FeBO_3$ [65].

Appendix B.2. Polycrystalline systems

In polycrystalline samples without texture one averages over all directions of the incident beam:

$$\frac{1}{4\pi}\int \mathrm{d}\vec{s}\,\tilde{D}(E,\vec{s}) = \sum_{\mu}\sum_{\nu} T^{\mu\nu}(E)\,\frac{1}{4\pi}\int \mathrm{d}\vec{s}\, s_\mu\, s_\nu. \tag{B.7}$$

The integral over all directions vanishes for the nondiagonal components of the tensor, while it is 1/3 for the diagonal components. This allows us to partly separate the summation over the vibrational modes from the sum over the resonant atoms in the unit cell [66], so that equation (B.1) then turns into:

$$\tilde{D}(E,\vec{s}) = \frac{1}{(2\pi)^3}\,\frac{V}{3N}\sum_j \int \mathrm{d}\vec{q}\,\delta(E-\hbar\omega_j(\vec{q}))\sum_m |\vec{s}\cdot\vec{e}_{j,m}(\vec{q})|^2. \tag{B.8}$$

For a monoatomic lattice the sum over all resonant atoms is of course identical to the sum over all atoms in the unit cell. That sum equals unity, by definition. Then the above expression merges into the exact definition of the DOS as given by equation (B.2).

References

[1] Jusserand B and Cardona M 1989 in *Topics in Applied Physics: Light Scattering in Solids V*, ed M Cardona and G Güntherodt (Berlin: Springer)

[2] Flik M I, Choi B I and Goodson K E 1992 *J. Heat Transfer* **114** 666

[3] Bushan B, Israelachvili J N and Landman U 1995 *Nature* **374** 607

[4] Gandhi M V and Thompson B S 1992 *Smart Materials and Structures* (Chapman and Hall: London)

[5] Kress W and de Wette F W 1991 *Surface Phonons* (Berlin: Springer)

[6] Khotkevich A V and Yanson I K 1995 *Atlas of Point Contact Spectra of Electron-Phonon Interactions in Metals* (Amsterdam: Kluwer)

[7] Nizzoli F and Sanderock J R 1990 *Dynamical Properties of Solids* Vol 6 (Amsterdam: North-Holland)
[8] Burkel E 1991 *Inelastic Scattering of X-Rays with Very High Energy Resolution* (Berlin: Springer)
[9] Burkel E 2000 *Rep. Prog. Phys.* **63** 171
[10] Burkel E and Sinn H 1994 *J. Phys.: Condensed Matter* **6** 225
[11] Sette F, Ruocco G, Krisch M, Masciovecchio C, Bergmann U, Mazzacurati V, Signorelli G and Verbeni R 1995 *Phys. Rev. Lett.* **75** 850
[12] Ruocco G, Sette F, Bergmann U, Krisch M, Masciovecchio C, Mazzacurati V, Signorelli G and Verbeni R 1996 *Nature* **379** 521
[13] Sinn H, Sette F, Bergmann U, Halcoussis C, Krisch M, Verbeni R and Burkel E 1997 *Phys. Rev. Lett.* **78** 1715
[14] Masciovecchio C, Monaco G, Ruocco G, Sette F, Cunsolo A, Krisch M, Mermet A, Soltwisch M and Verbeni R 1998 *Phys. Rev. Lett.* **80** 544
[15] Seto M, Yoda Y, Kikuta S, Zhang X W and Ando M 1995 *Phys. Rev. Lett.* **74** 3828
[16] Sturhahn W, Toellner T S, Alp E E, Zhang X, Ando M Yoda Y, Kikuta S, Seto M, Kimball C W and Dabrowski B 1995 *Phys. Rev. Lett.* **74** 3832
[17] Chumakov A I, Rüffer R, Grünsteudel H, Grünsteudel H F, Grübel G, Metge J, Leupold O and Goodwin H A 1995 *Europhys. Lett.* **30** 427
[18] Chumakov A I and Sturhahn W 1999 *Hyperfine Interact.* **123/124** 781
[19] Singwi K S and Sjölander A 1960 *Phys. Rev.* **120** 1093
[20] Visscher W M 1960 *Ann. Phys.* **9** 194
[21] Toellner T S, Hu M Y, Sturhahn W, Quast K and Alp E E 1997 *Appl. Phys. Lett.* **71** 2112
[22] Chumakov A I, Barla A, Rüffer R, Metge J, Grünsteudel H F, Grünsteudel H, Plessel J, Winkelmann H and Abd-Elmeguid M M 1998 *Phys. Rev. B* **58** 254
[23] Hu M Y, Toellner T S, Sturhahn W, Hession P M, Sutter J P and Alp E E 1999 *Nucl. Instrum. Methods* A **430** 271
[24] Mooney T M, Toellner T S, Sturhahn W, Alp E E and Shastri S D 1994 *Nucl. Instrum. Methods* A **347** 348
[25] Kishimoto S 1991 *Nucl. Instrum. Methods* A **309** 603
[26] Baron A Q R 1995 *Nucl. Instrum. Methods* A **352** 665
[27] Stevens J G and Stevens V E 1973 *Mössbauer Effect Data Index* (New York: Plenum)
[28] Chumakov A I, Rüffer R, Baron A Q R, Grünsteudel H, Grünsteudel H F and Kohn V G 1997 *Phys. Rev.* B **56** 10758
[29] Kohn V G, Chumakov A I and Rüffer R 1998 *Phys. Rev.* B **58** 8437
[30] van Hove L 1954 *Phys. Rev.* **95** 249
[31] Marshall W and Lovesey S W 1971 *The Theory of Thermal Neutron Scattering* (London: Oxford University Press)
[32] Lipkin H J 1960 *Ann. Phys.* **9** 332
[33] Lipkin H J 1995 *Phys. Rev.* B **52** 10073
[34] Bedzyk M J, Bommarito G M and Schildkraut J S 1989 *Phys. Rev. Lett.* **62** 1376
[35] Krol A, Sher C J and Kao Y H 1988 *Phys. Rev.* B **38** 8579
[36] Wang Y, Bedzyk M and Caffrey M 1992 *Science* **258** 775
[37] Dev B N, Das A K, Dev S, Schubert D W, Stamm M, and Materlik G 2000 *Phys. Rev.* B **61** 8462
[38] Röhlsberger R 1999 *Hyperfine Interactions* **123/124** 301
[39] Feng Y P, Sinha S K, Deckman H W, Hastings J B and Siddons D P 1993 *Phys. Rev. Lett.* **71** 537
[40] Röhlsberger R, Sturhahn W, Toellner T S, Quast K W, Hession P M, Hu M Y, Sutter J P and Alp E E 1999 *J. Appl. Phys.* **86** 584
[41] Minkiewicz V J, Shirane G and Nathans R 1967 *Phys. Rev.* **162** 528
[42] Schober H R and Dederichs P H 1981 in *Phonon States of Elements, Electron States and Fermi Surfaces of Alloys* ed K H Hellwege and J L Olsen, Landolt Börnstein, New Series, III/13a (Berlin: Springer)
[43] Fåk B and Dorner B 1992 *Institut Laue Langevin Technical Report* No 92FA008S, unpublished
[44] Fultz B, Ahn C C, Alp E E, Sturhahn W and Toellner T S 1997 *Phys. Rev. Lett.* **79** 937
[45] Glyde H R and Svensson E C 1987 in *Methods of Experimental Physics* Vol 23 B, ed D L Price and K Sköld (New York: Academic)
[46] Dorner B 1982 *Coherent Inelastic Neutron Scattering in Lattice Dynamics* (Berlin: Springer)
[47] Kodama R H and Edelstein A S 1999 *J. Appl. Phys.* **85** 4316
[48] Sun S, Murray C B, Weller D, Folks L and Moser A 2000 *Science* **287** 1989
[49] Padovani S, Chado J, Scheurer F and Bucher J P 1999 *Phys. Rev.* B **59** 1887
[50] Bode M, Pascal R and Wiesendanger R 1997 *J. Vac. Sci. Techn.* A **15** 1285
[51] Sturhahn W 1999 private communication
[52] Sturhahn W, Röhlsberger R, Alp E E, Ruckert T, Schrör H and Keune W 1999 *J. Magn. Magn. Mater.* **198–199**

590
[53] Röhlsberger R, Sturhahn W, Toellner T S, Quast K W, Alp E E, Bernhard A, Metge J, Rüffer R Burkel E 1999 *Physica* B **263–264** 581
[54] Tolbert W A, Dennis W M and Yen W M 1990 *Phys. Rev. Lett.* **65** 607
[55] Hu M Y, Sturhahn W, Toellner T S, Hession P M, Sutter J P and Alp E E 1999 *Nucl. Intrum. Methods* A **428** 551
[56] Sturhahn W 2000 *Hyperfine Interact.* **125** 149
[57] Kohn V G and Chumakov A I 2000 *Hyperfine Interact.* **125** 205
[58] Johnson D W and Spence J C H 1974 *J. Phys. D: Appl. Phys.* **7** 771
[59] Fultz B, Stephens T A, Alp E E, Hu M Y, Sutter J P, Toellner T S and Sturhahn W 2000 *Phys. Rev.* B **61** 14517
[60] Sturhahn W and Toellner T S 2000 unpublished
[61] Brandt R A, Coddens G, Chumakov A I and Calvayrac Y 1999 *Phys. Rev.* B **59** 14145
[62] Ashcroft N W and Mermin N D 1976 *Solid State Physics* (Philadelphia: Holt-Saunders)
[63] Rose M E 1957 *Elementary Theory of Angular Momentum* (New York: Wiley)
[64] Sturhahn W and Kohn V G 1999 *Hyperfine Interact.* **123/124** 367
[65] Hession P M, Sturhahn W, Alp E E, Toellner T S, Metcalf P, Hu M Y, Sutter J P and Mullen J P 2000 unpublished
[66] Chumakov A I, Rüffer R, Leupold O, Barla A, Thiess H, Jil J M, Alberto H V, Vilão R C, Ayres de Campos N, Kohn V G, Gerken M and Lucht M 2001 *Phys. Rev.* B **63** 172301